VIRTUAL AND PHYSICAL PROTOTYPING
2025, VOL. 20, NO. 1, e2499934 (21 pages)
https://doi.org/10.1080/17452759.2025.2499934

Enhanced mechanical properties and reduced anisotropy of material extrusion-manufactured short carbon fibre-reinforced plastic via cold isostatic pressing

Sangjun Jeon[a,b], Seong Je Park[b,c], Seung Ki Moon[b,c] and Daejong Yang[a,d]

[a]Department of Future Convergence Engineering, Kongju National University, Cheonan, Republic of Korea; [b]School of Mechanical and Aerospace Engineering, Nanyang Technological University, Singapore, Singapore; [c]Singapore Centre for 3D Printing, School of Mechanical and Aerospace Engineering, Nanyang Technological University, Singapore, Singapore; [d]Department of Mechanical and Automotive Engineering, Kongju National University, Cheonan, Republic of Korea

ABSTRACT

The increasing adoption of short carbon fibre-reinforced plastics (sCFRP) manufactured through material extrusion (MEX) in high-value-added industries has driven the development of various post-processing methods to enhance MEX-manufactured sCFRP mechanical properties. However, conventional post-processing methods require high temperatures and extended processing times, leading to potential polymer degradation. This study presents a novel room-temperature approach using cold isostatic pressing (CIP) to enhance mechanical properties with reduced anisotropy in MEX-manufactured sCFRP components. The effects of various CIP pressures (250-1000 bar) on the mechanical properties were evaluated through tensile, flexural and interlaminar shear strength (ILSS) tests. Additionally, mechanical anisotropy was assessed using tensile tests at different raster angles (0°, 90°) before and after CIP treatment. The mechanical properties significantly improved after CIP treatment, with the optimal pressure of 500 bar, resulting in a 103% increase in tensile strength for 0° raster angle specimens and a 143.3% increase for 90° specimens, effectively reducing the anisotropy from 77.3% to 42.1%. Microstructural analysis revealed reduced voids and enhanced layer adhesion with increased crystallinity. CIP-treated sCFRP maintained excellent dimensional stability within a 3% variation. This study demonstrates the potential of room-temperature CIP as a post-processing method for improving the mechanical properties of MEX-manufactured composites.

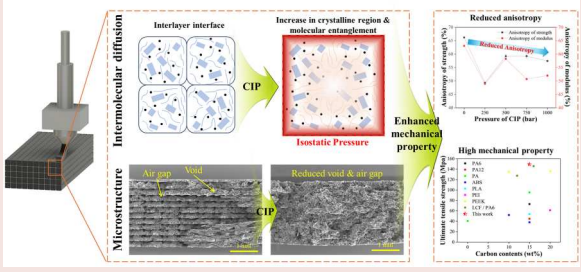

ARTICLE HISTORY
Received 26 February 2025
Accepted 13 April 2025

1. Introduction

Global environmental regulations have been driving the demand for lightweight materials in mobility and aerospace applications to reduce component weight and improve efficiency [1–3]. This trend has driven extensive research into composite materials as alternatives to conventional steel [4,5]. Carbon fibre-reinforced plastic (CFRP) contributes to environmental sustainability through weight reduction offering distinctive properties of high strength, high modulus, and low density [6–8]. The global usage of CFRP has grown rapidly at an annual rate of approximately 12.5% over the past two decades, leading to substantial End-of-Life waste accumulation [9]. This rapid growth, coupled with increasing environmental concerns, necessitates developing manufacturing processes that minimise material waste during CFRP production [10].

Material extrusion (MEX) is widely used in the automotive and aerospace industries for composite manufacturing due to its cost-effective and minimal waste

CONTACT Seung Ki Moon skmoon@ntu.edu.sg School of Mechanical and Aerospace Engineering, Nanyang Technological University, Singapore 639798, Singapore; Singapore Centre for 3D Printing, School of Mechanical and Aerospace Engineering, Nanyang Technological University, Singapore 639798, Singapore; Daejong Yang daejong@kongju.ac.kr Department of Future Convergence Engineering, Kongju National University, Cheonan 31080, Republic of Korea; Department of Mechanical and Automotive Engineering, Kongju National University, Cheonan 31080, Republic of Korea

nature [11,12]. Short carbon fibre-reinforced plastic (sCFRP) offers superior processability and ecological benefits compared to continuous carbon fibre-reinforced plastic [13,14]. However, MEX-manufactured sCFRP has inherent limitations due to the discontinuous deposition process [15]. The layer-by-layer fabrication results in weakened interlayer bonding and void formation, which significantly deteriorate mechanical properties [16–18]. Moreover, MEX-manufactured sCFRP exhibits significant mechanical anisotropy. The mechanical strength of MEX-manufactured sCFRP components is significantly lower in the perpendicular (90°) direction than in the horizontal nozzle (0°) direction [19]. This directional dependency of mechanical behaviour is due to the alignment of polymer chains and carbon fibres (CFs) along the deposition direction during MEX [20]. The reduced mechanical properties limit MEX-manufactured sCFRP applications in aerospace and automotive sectors where high strength and reliability are critical [21]. For instance, aerospace applications typically require void content below 1% and low mechanical strength variations for structural components [22].

The mechanical properties of MEX-manufactured components are considerably influenced by printing parameters including nozzle temperature, printing speed, layer height, and raster angle [23,24]. Numerous studies have conducted printing parameter optimisation to enhance mechanical properties and interlayer bonding [25]. Gómez-Ortega et al. investigated the effects of printing parameters on sCFRP mechanical properties, reporting optimal conditions of nozzle temperature and infill rate for maximum tensile strength [26]. Similarly, Rimašauskas et al. demonstrated that reducing layer height from 0.4 mm to 0.3 mm decreased void volume from 27.5% to 18.5% [27]. Despite optimisation of MEX parameters such as nozzle temperature, printing speed, and layer height, the mechanical characteristics remain fundamentally limited by void formation and weak interlayer bonding. Voids formed during the printing process act as stress concentrators, leading to significant reduction in mechanical strength and fatigue resistance [28]. In layer-by-layer manufacturing process, restricted molecular diffusion and entanglement between adjacent layers, primarily caused by rapid cooling and insufficient contact time, result in weak interlayer bonding [29]. These limitations necessitate additional post-processing methods to enhance mechanical performance.

Post-processing through thermal treatment has been widely investigated as a potential solution [30–32]. This approach enhances mechanical behaviour through polymer chain rearrangement and diffusion above glass transition temperature (T_g) [33]. As a result, annealing reduces residual stresses and improves interlayer bonding properties by eliminating internal defects [34,35]. Peng Wang et al. investigated the effects of annealing time and temperature on the mechanical properties and interlaminar shear strength (ILSS) of MEX-manufactured composites [36]. This result showed that the annealing process decreased the internal defects and increased crystallinity of composite. K. Wang et al. reported that thermal treatment at the optimal temperature (100°C) for 8 h led to enhanced dimensional stability and improved mechanical properties [37]. Therefore, annealing plays a vital role in enhancing the properties of MEX-manufactured composites. However, annealing requires high temperatures for polymer recrystallization and interlayer rebonding, leading to significant energy consumption and potential polymer degradation from extended processing time.

Combined heat and pressure post-processing methods have been developed to enhance molecular diffusion while reducing processing time. J. Wang et al. investigated conventional hot-pressing at 200°C and 0.841 MPa, showing improved interfacial bonding strength and toughness compared to the non-treated samples [38]. Andreu et al. studied the enhancement of interlayer bonding strength by incorporating a hot roller system into the MEX printer [29]. While the high-pressure roller contact increased the bonding area between filaments and improved mechanical properties, the direct application of heat and pressure caused surface delamination of the components. The non-uniform pressure distribution in both hot-pressing and roller-based methods can lead to internal stress concentrations, resulting in warpage and dimensional inaccuracies.

To achieve uniform pressure distribution, researchers have investigated various approaches. W. Wu et al applied hot isostatic pressing (HIP) at 360°C and 10 MPa, achieving 384% improvement in interlayer strength without geometric distortion [39]. However, the high temperature and pressure processing required substantial energy input. As an alternative approach, Park et al. developed the warm isostatic press (WIP) process, demonstrating 16.3% ultimate tensile strength enhancement at lower temperatures (130°C) [40]. Nevertheless, the elevated processing temperature and extended processing time exceeding one hour led to polymer deterioration and high energy consumption [41]. A comparison of various post-processing methods including processing parameters and conditions is summarised in Table 1. As shown in Table 1, conventional thermal and pressure-based methods require high temperature and extended processing time, which can lead to polymer degradation and high energy consumption.

Table 1. Comparison of various post-processing methods for MEX-manufactured sCFRP.

Method	Temperature	Pressure	Processing Time	Advantages	Disadvantages	References
Annealing	150–200°C	N/A	2–8 h	Simple process	Long processing time	Wang et al. [37]; Yu et al. [34]
Hot Press	100–200°C	Below 10 bar	Below 0.5 h	Short processing time	Dimensional inaccuracies, Warpage	Wang et al. [38]; Mei et al. [42]
HIP	200–400°C	50 MPa	1–2 h	Uniform pressure, good densification	High energy consumption	Wu et al. [39]
WIP	100–200°C	50 bar	1–2 h	Lower temperature	High energy consumption	Seong Jun Park et al. [19]
CIP	Room Temperature	250–1000 bar	0.5 h	No thermal damage, short processing time		This work

Cold isostatic pressing (CIP) offers a promising alternative approach. The CIP process applies uniform pressure in all directions, improving density and microstructural uniformity while minimising shape distortion compared to uniaxial pressing [43]. The CIP process utilises a hydrostatic pressure transmission medium to apply uniform high-pressure conditions at room temperatures [44]. The uniform pressure distribution facilitates component densification by increasing interlayer contact area and removing internal voids [45]. Additionally, CIP can be applied to components with complex geometries and can improve material characteristics without thermal deformation or degradation [46]. These CIP characteristics are expected to be highly suitable for improving the interlayer bonding strength of MEX-manufactured sCFRP components. However, the effect of CIP post-processing on the mechanical behaviour of MEX-manufactured sCFRP remains to be explored.

This study aimed to investigate the potential of CIP as a novel room-temperature post-processing method to enhance the mechanical properties of MEX-manufactured sCFRP components. Compared to conventional thermal treatments that require high temperatures and extended processing times, the CIP approach applies uniform isostatic pressure at room temperature, maintaining dimensional stability without polymer degradation while reducing processing time. This work specifically focuses on utilising isostatic pressure to strengthen interfacial molecular bonding while simultaneously eliminating process-induced voids in the components. First, mechanical behaviour analysis is conducted using a custom-designed chamber to assess the effects of various isostatic pressures (250–1000 bar) through tensile, flexural, and interlaminar shear tests. This includes comprehensive analysis of pressure-dependent anisotropy reduction between different raster angles (0° and 90°). Additionally, differential scanning calorimetry (DSC) analysis is conducted to investigate the effect of the isostatic pressure treatment on the thermal properties and crystallization behaviour. The effect of the isostatic pressure post-treatment is further investigated through a dimensional and morphological analysis of the post-treated specimens. Finally, a comprehensive analysis of the pressure-induced bonding mechanisms and structural modifications is presented to establish the fundamental relationships between process parameters, microstructural changes, and mechanical performance. The findings of this study are expected to establish CIP as an industrially viable post-processing method for MEX-manufactured sCFRP components, potentially enabling their widespread adoption in high-performance applications.

2. Materials and methods

2.1. Fabrication of specimens

Polyamide (PA) was selected as the matrix material due to its superior mechanical properties, thermal stability, and chemical resistance, which makes it a preferred matrix for sCFRP in automotive and aerospace industries where high-performance lightweight components are essential [47]. For this study, Ultrafuse PAHT CF 15 (BASF, Germany), a high-temperature PA-based filament containing 15% sCFs, was used to fabricate the specimens [48]. As shown in Figure 1(a), the specimen fabrication was conducted using an Epsilon W50 (BCN3D, Netherlands) MEX equipment, with the following process parameters [49–51]: (i) a printing speed of 30 mm/s, (ii) extruder nozzle temperature: 260°C, (iii) build plate temperature: 90°C, (iv) layer thickness: 0.25 mm, and (v) infill density: 100%. The mechanical testing configurations and specimens are presented in Figure 1(b,c), where tensile, flexural, and interlaminar shear specimens were fabricated according to ASTM 638, 790, 2344 standards, respectively. To evaluate anisotropy and interlayer strength, tensile specimens were fabricated in 0° and 90° directions, respectively. The detailed specimen information is illustrated in Figure 1.

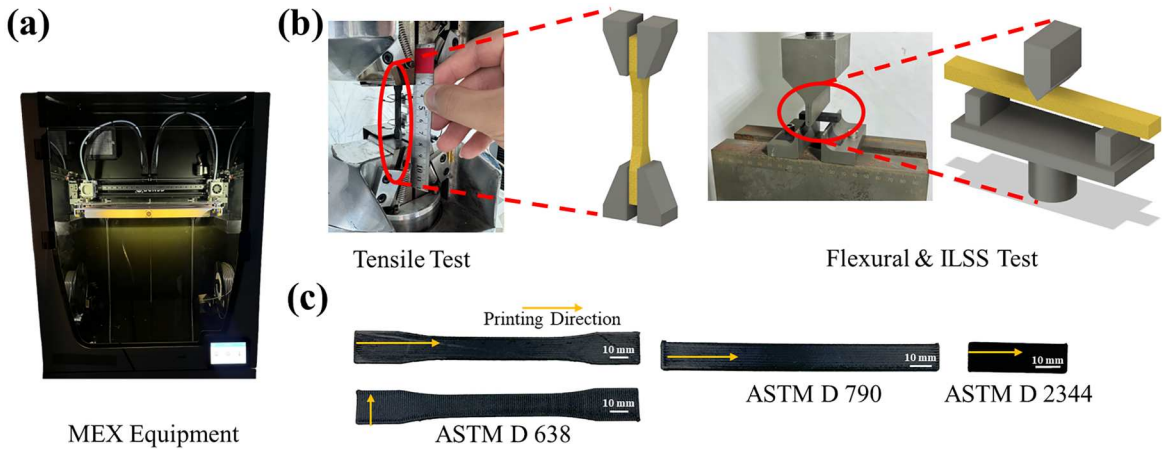

Figure 1. Schematic illustration of the specimen fabrication process: (a) MEX equipment, (b) mechanical test, and (c) mechanical test specimens.

2.2. Cold isostatic pressing

The CIP was employed to uniformly compress the sCFRP specimens under high hydrostatic pressure. Figure 2(a) exhibits the schematic diagram of CIP process. Prior to treatment, specimens were vacuum-sealed in a polyimide film to minimise internal pressure [52]. As shown in Figure 2(b), the CIP was conducted using a custom-built chamber equipped with a control system capable of isostatic pressing up to 3000 bar. The CIP process was performed at room temperature. The chamber was filled with fluid medium, and compression was applied at a rate of 2 bar/s until reaching the target isostatic pressures (250, 500, 750, or 1000 bar). Figure 2(c) presents the time–pressure profiles for these conditions. It was held at each target pressure for 5 min to ensure uniform isostatic compression. Following treatment, the system was gradually returned to initial pressure. Both compression and decompression rates were controlled to minimise internal stresses and microdefects in the specimens.

2.3. Mechanical testing

Mechanical properties were evaluated through tensile, flexural, and interlaminar shear strength (ILSS) tests. Tensile tests were conducted using an MTS 810 testing machine (MTS, US) following ASTM D638 Type 1 specifications, with a 100 kN load cell and a constant crosshead displacement of 2 mm/min. Flexural tests were carried out on an AG-X testing machine (Shimadzu, Japan) according to ASTM D790 standards, with a 50 kN load cell and a constant crosshead displacement rate of 2 mm/min. ILSS tests were performed using an ST-1001 testing machine (Salt, Republic of Korea) following ASTM D2344 specifications, with a 100 kN load cell and a constant crosshead displacement of 1 mm/min.

2.4. Thermal and crystallinity analysis

DSC analysis was conducted using a DSC Q20 (TA Instruments, US) to investigate thermal characteristics and crystallinity changes in MEX-manufactured sCFRP following isostatic pressure post-treatment. Prior to testing, samples were dried at 100°C for 6 h to prevent moisture-induced thermal degradation of the components [52]. The dried samples were subjected to a heating cycle from 30°C to 250°C at a rate of 10°C/min and cooled at the same rate under a nitrogen atmosphere. The degree of crystallinity (X_c) was calculated using Equation (1).

$$X_c = \left(\frac{\Delta H_{exp}}{\varphi \times \Delta H^{\circ}} \right) \times 100\ \% \quad (1)$$

where ΔH_{exp} is the experimentally measured crystallization enthalpy, φ is the content of PA matrix, and ΔH° is the reported enthalpy change of 100% crystallization of polyamide [47].

2.5. Morphology analysis and dimensional measurements

Scanning electron microscopy (SEM) was employed to analyse the morphological changes of MEX-manufactured sCFRP at different isostatic pressure conditions. Fracture surfaces of tested tensile specimens were investigated using a VEGA3 (TESCAN, Czech Republic). The dimensional accuracy was evaluated before and after CIP treatment according to the ISO 527-1:2012 standard. Specimen length and thickness were measured at three points using Vernier calipers, with the average values used for subsequent tensile, flexural, and ILSS calculations.

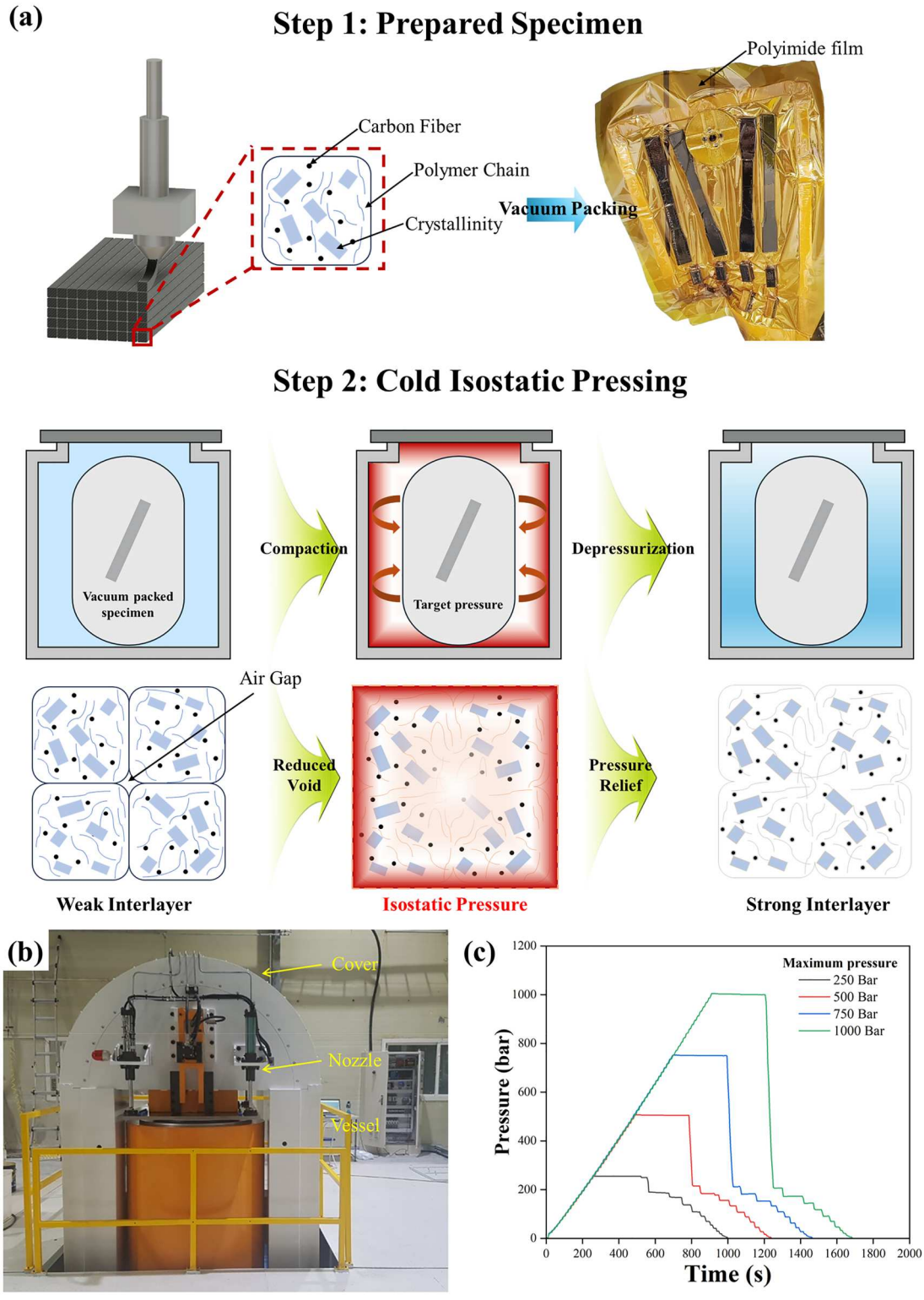

Figure 2. CIP experimental setup and process parameters: (a) Schematic of CIP process, (b) Large-scale CIP equipment, and (c) Time–pressure profiles for different pressure conditions.

3. Results

3.1. Effects of the CIP process on the sCFRP mechanical properties

The mechanical properties of sCFRP were evaluated to assess the effectiveness of CIP post-treatment under different isostatic pressure conditions. Figure 3(a) demonstrates the relationship between ultimate tensile strength and isostatic pressure for specimens fabricated with 0° raster angle. The ultimate tensile strength of the sCFRP components shows a gradual enhancement with increasing isostatic pressure. The untreated specimens exhibited 73 MPa, while the post-treated sCFRP with 500 bar increased the maximum tensile strength to 149.3 MPa, representing a 104.5% improvement. Although specimens treated at elevated pressures (750 and 1000 bar) showed slightly decreased strength, these post-treated specimens retained superior performance compared to untreated specimens. Similarly, sCFRP fabricated with 90° raster angle exhibited comparable behaviour, as shown in Figure 3(b). The ultimate tensile strength increased from 24.8 to 60.9 MPa with 500 bar treatment, demonstrating a 145% improvement. Furthermore, the tensile modulus also showed significant enhancement with CIP treatment, as illustrated in Figure 3(a,b). For specimens with 0° raster angle, the tensile modulus increased from 7.2 to 10.1 GPa at 500 bar, while specimens with 90° raster angle showed an increase from 3.6 to 4.4 GPa. The observed enhancements in tensile strength and modulus across both raster angles demonstrate the effectiveness of CIP treatment in improving the overall tensile performance of MEX-manufactured sCFRP specimens.

MEX-manufactured parts inherently exhibit high anisotropy, resulting in weaker mechanical properties perpendicular to the printing direction. Therefore, it is essential to evaluate the effects of post-treatment processing on anisotropy. To investigate the impact of CIP treatment on this directional dependency, anisotropy was calculated using the tensile strength according to Equation (2) [19].

$$\text{Anisotropy} = \left(\frac{\sigma_0 - \sigma_{90}}{\sigma_0}\right) \times 100\% \qquad (2)$$

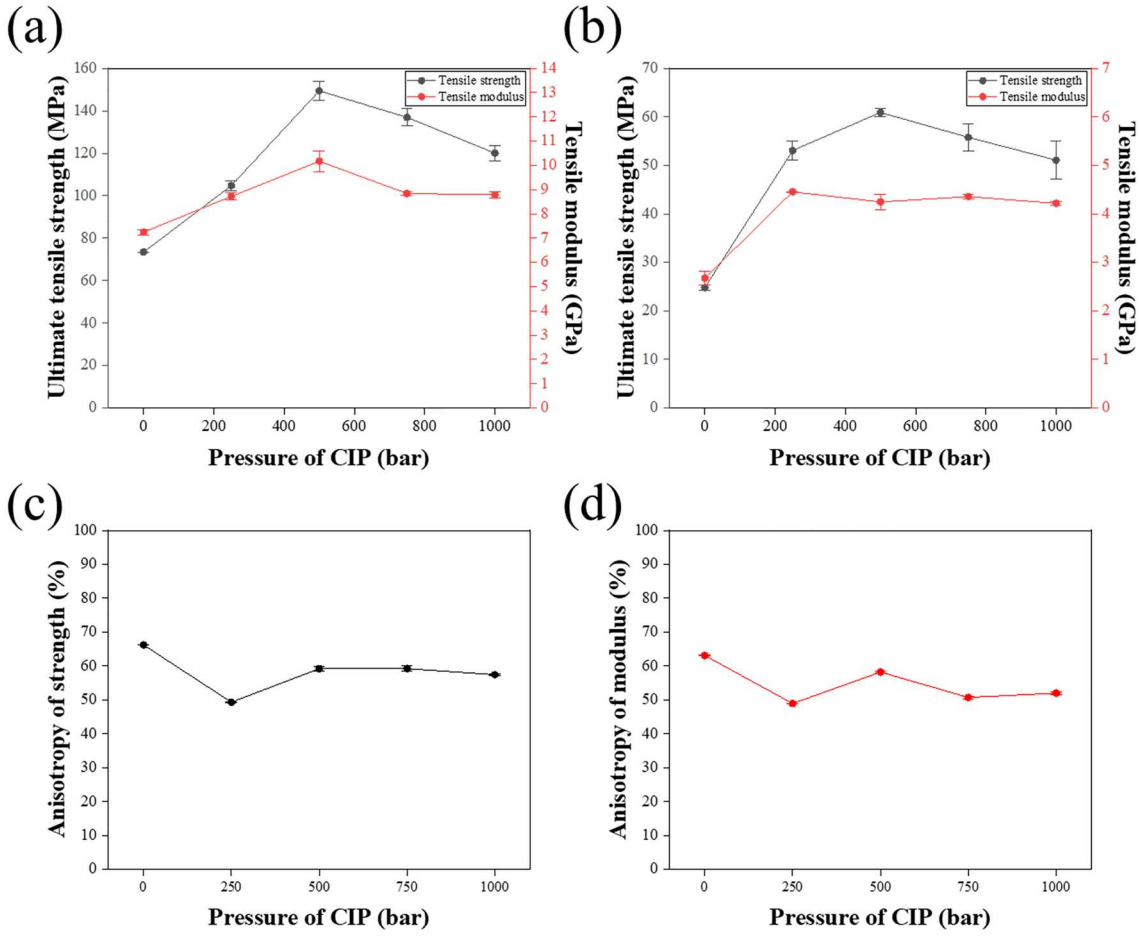

Figure 3. Tensile properties of CIP-treated sCFRP specimens under different pressure conditions: (a) 0° raster angle, (b) 90° raster angle, (c) Anisotropy of tensile strength and (d) Anisotropy of modulus.

where σ_0 and σ_{90} represent the experimentally measured ultimate tensile strengths for specimens with 0° and 90° raster angles, respectively.

Figure 3(c,d) presents the anisotropy of tensile strength and modulus as a function of CIP pressure. The untreated specimens exhibited a tensile strength anisotropy of 66%, which can be attributed to the inherent structural characteristics of MEX-manufactured parts. In contrast, the CIP-treated sCFRP specimens demonstrated reduced mechanical anisotropy compared to untreated specimens. As shown in Figure 3(c), the tensile strength anisotropy reached the optimal its value of 49% at 250 bar. Similarly, the tensile modulus observed reduced anisotropy with isostatic pressure treatment (Figure 3(d)). The observed reductions in both tensile strength and modulus anisotropy demonstrate that CIP treatment enhances the overall structural integrity of MEX-manufactured sCFRP parts through improved interfacial bonding.

Additional mechanical tests including flexural and interlaminar shear tests were conducted to evaluate the effects of CIP post-treatment comprehensively. Following the superior tensile strength observed in tensile test results, specimens with 0° raster angle were selected for subsequent mechanical characterisation. Figure 4(a) presents the flexural properties evaluated under various isostatic pressures. Similar to the tensile behaviour, flexural strength showed enhancement after CIP treatment. The ultimate flexural strength improved from 139.1 to 195.9 MPa at 500 bar. However, specimens treated at elevated pressures showed a slight decrease in flexural properties. The specimens treated at 750 and 1000 bar exhibited flexural strengths of 149.5 and 104.9 MPa, respectively, maintaining superior performance compared to untreated specimens. The flexural modulus also demonstrated comparable pressure-dependent behaviour, reaching from 11.1 to 15.1 GPa at 500 bar. Despite the slight decrease in flexural modulus above 500 bar, CIP-treated specimens maintained approximately 30% improvement compared to untreated specimens.

The ILSS was evaluated under various CIP conditions to assess the CIP treatment effectiveness on interlayer bonding. The ILSS were calculated from the load responses using Equation (3) and are depicted in Figure 4(b) [53].

$$\tau = 0.75 \times \frac{P_{max}}{(w \times t)} \tag{3}$$

where τ is the short-beam strength or apparent ILSS (MPa), P_{max} is the maximum load observed during the test (N), w is the specimen width (mm), and t is the specimen thickness (mm).

The CIP treatment significantly enhanced the interlayer bonding increasing from 11.5 MPa for untreated specimens to 21 MPa at 500 bar (82% improvement). While ILSS showed a slight decrease at elevated isostatic pressures above 500 bar, the treated specimens still maintained 14% higher values compared to untreated specimens. These results confirm that post-processing using the CIP method successfully improves the mechanical performance of MEX-manufactured sCFRP specimens through enhanced interfacial and interlayer bonding.

3.2 CIP effects on the thermal properties and crystallinity of sCFRP

The thermal characteristics and crystallinity of semi-crystalline polymers are crucial material properties that determine polymer structure [54]. The X_c particularly influences mechanical behaviour, leading to improved strength and stiffness while resulting in greater brittleness [55]. In sCFRP, X_c affects both the matrix's

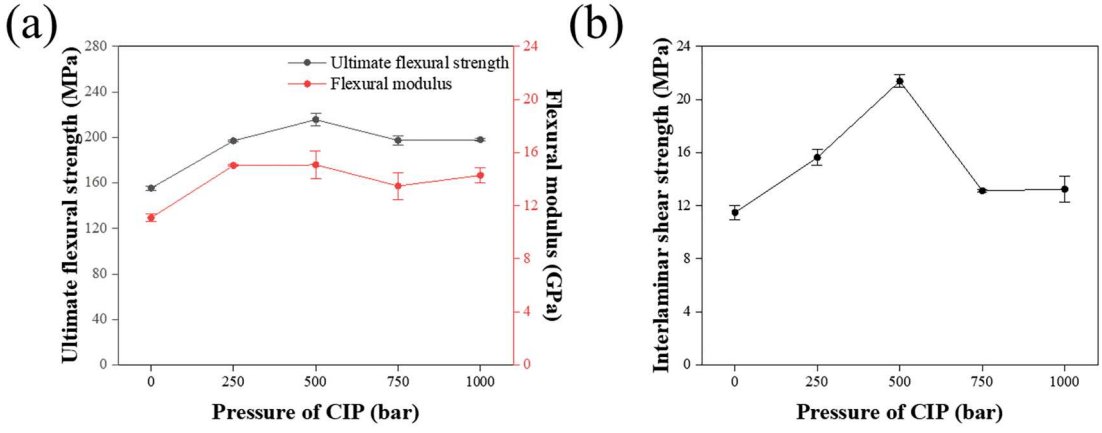

Figure 4. Mechanical characterisation of CIP-treated sCFRP specimens: (a) Ultimate flexural strength and modulus and (b) ILSS value.

mechanical strength and the CF-matrix interfacial bonding [56]. To investigate the impact of CIP post-treatment on the thermal properties and crystallinity of sCFRP components, DSC analysis was conducted.

Figure 5 presents the DSC heating curves for sCFRP specimens at different CIP conditions, with the corresponding thermal properties summarised in Table 2. The untreated specimen exhibited a X_c of 26.82%, which increased to 30.15% at 250 bar. The X_c reached its peak value of 30.43% (12.4% enhancement) at 500 bar, followed by a slight decrease to 30.40% and 28.62% at 750 and 1000 bar, respectively. This variation in X_c can be attributed to pressure-induced molecular chain alignment and enhanced nucleation.

The glass transition temperature (T_g) also exhibited pressure-dependent behaviour with isostatic pressure treatment. The T_g increased from 73.11°C in untreated specimens to 74.93°C at 500 bar, indicating enhanced molecular chain rigidity. At elevated isostatic pressures, T_g slightly decreased to 73.40°C and 73.46°C at 750 and 1000 bar, respectively. These variations in thermal properties suggest alterations in molecular chain mobility and rigidity within the polymer matrix. Notably, CIP achieved polymer recrystallization at room temperature, demonstrating its potential as an effective post-processing method for MEX-based manufacturing.

3.3. Effects of CIP process parameters on the microstructural characteristics of sCFRP

MEX-manufactured components are fabricated through sequential deposition of extruded filaments. The discontinuous layering process leads to void formation at the interfaces between adjacent deposited lines [31]. These voids significantly affect the internal porosity and microstructure of manufactured components, resulting in reduced mechanical properties [57].

Table 2. Mechanical properties of specimens to different sintering temperatures.

Specimen	T_g (°C)	X_c (%)
0 bar	73.11	26.82
250 bar	72.68	30.15
500 bar	74.93	30.43
750 bar	73.40	30.40
1000 bar	73.46	28.62

Morphological analysis was conducted using SEM to investigate the interlayer bonding characteristics of specimens subjected to various isostatic pressures. Figure 6 presents the fracture surface morphology of specimens with a 0° raster angle. As shown in Figure 6(a), the tensile fractured surfaces of untreated specimens show uniformly distributed CF and voids between deposited filaments. Small voids were observed due to CF extraction during the fabrication of sCFRP components. Furthermore, untreated specimens exhibited triangular inter-filament voids due to the extrusion process. In contrast, CIP-treated sCFRP specimens showed progressively decreased voids with increasing isostatic pressure from 250 bar to 1000 bar (Figure 6(c–i)). The increasing pressure also enhanced interlayer contact areas. The specimens treated at 1000 bar demonstrated superior interlayer bonding through the elimination of interlayer interfaces. To compare the microstructural characteristics at different raster angles, Figure 7 illustrates the fracture surface morphology of specimens with 90° raster angle. Untreated specimens exhibited CF alignment along the nozzle direction (Figure 7(a)), leading to significant mechanical anisotropy. The microstructural changes observed in Figure

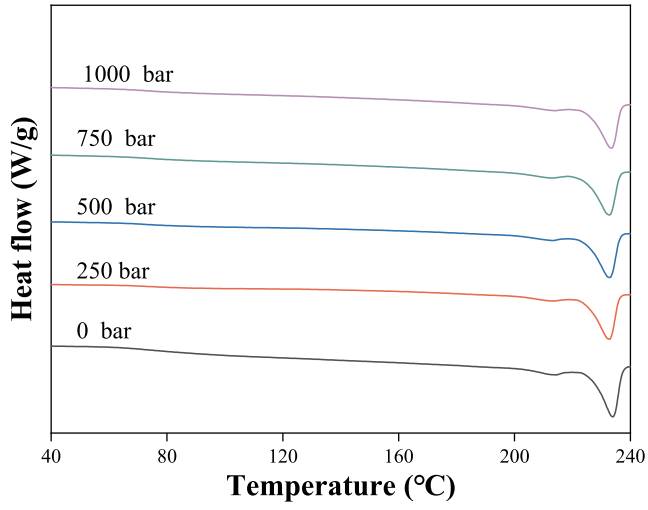

Figure 5. DSC heating curves for untreated and CIP-treated specimens at different pressures.

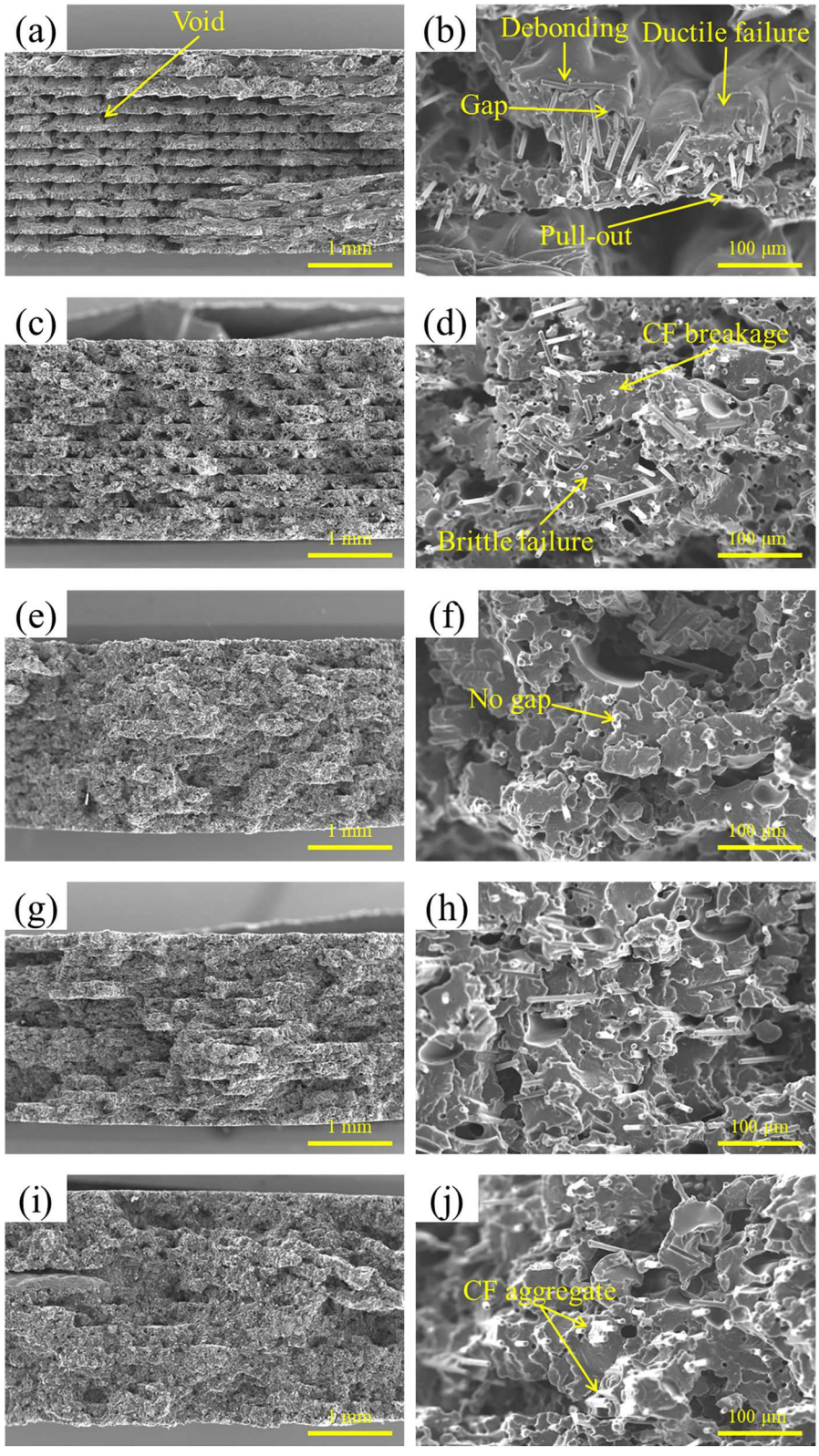

Figure 6. SEM micrographs of fracture surfaces for 0° raster angle specimens post-treated in (a)(b) 0 bar, (c)(d) 250 bar, (e)(f) 500 bar, (g)(h) 750 bar and (i)(j) 1000 bar.

7(c–j) shows that CFs gradually developed random orientation distributions with increasing CIP pressure, which corresponded to the reduction in mechanical anisotropy previously discussed in Section 3.1. The increased pressure promoted enhanced interlayer adhesion through improved interfacial contact.

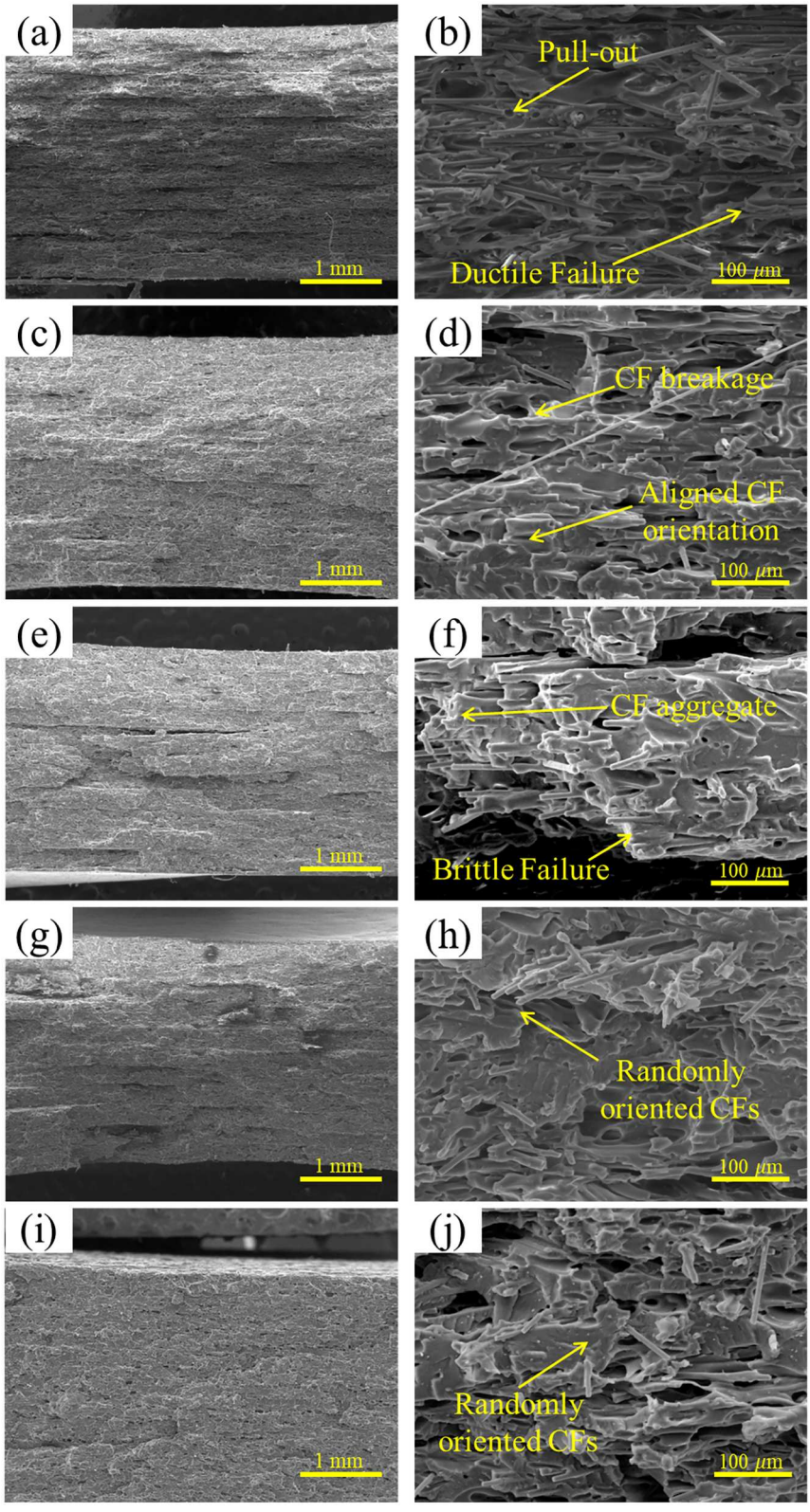

Figure 7. SEM micrographs of fracture surfaces for 90° raster angle specimens post-treated in (a)(b) 0 bar, (c)(d) 250 bar, (e)(f) 500 bar, (g)(h) 750 bar and (i)(j) 1000 bar.

The fracture behaviour exhibited distinct characteristics depending on the raster angle orientation. For specimens with a 0° raster angle, CF pull-out was the dominant failure mode, while specimens with a 90° primarily showed matrix fracture. This difference in failure modes resulted from the load-bearing direction relative

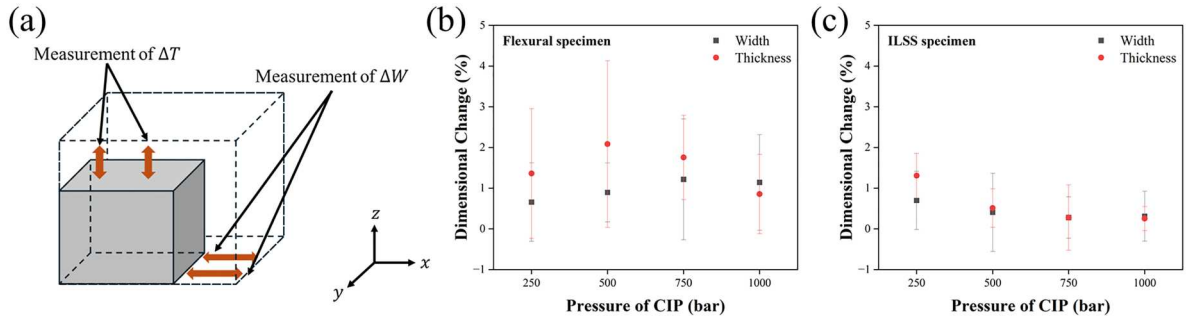

Figure 8. Dimensional stability analysis of width and thickness for the sCFRP under different pressure conditions: (a) Measurement locations on specimens, (b) Dimensional variations of Flexural specimens and (c) ILSS specimens.

to CF orientation [58]. The CIP treatment significantly influenced these failure mechanisms. Untreated specimens showed weak fibre-matrix interfacial bonding with extensive fibre debonding and pull-out, regardless of raster angle orientation (Figures 6(b)). However, after CIP treatment at 500 bar, specimens demonstrated enhanced fibre-matrix adhesion evidenced by CF breakage rather than pull-out (Figure 6(f)). This improvement in tensile properties can be attributed to enhanced load-bearing capability of CF in the polymer matrix through improved interfacial bonding.

The CIP treatment induced significant microstructural modifications, leading to enhanced component densification and improved fibre-matrix interfacial bonding. The enhanced densification, coupled with improved fibre-matrix interfacial bonding, significantly improved mechanical properties while reducing the directional dependency of the material behaviour.

3.4. Dimensional accuracy

Post-processing treatments often result in specimen deformation, which can significantly affect the dimensional accuracy and functional performance of manufactured components. To evaluate dimensional stability, sCFRP specimens were measured before and after CIP processing, as shown in Figure 8. Specimen width and thickness measurements were taken using Vernier callipers (Figure 8(a)). The specimens exhibited different deformation rates under varying isostatic pressures due to void reduction within the composite. Figure 8(b) shows that dimensional changes in flexural specimens remained within 1–4%, and changes of up to 2% were observed for ILSS specimens in Figure 8(c). An examination of the deformation rates and standard deviations confirmed minimal dimensional variations under all pressure conditions.

The slightly higher deformation observed in flexural specimens compared to ILSS specimens can be attributed to the flexural specimens larger dimensions and corresponding void content. The uniform pressure distribution during CIP treatment maintained geometric consistency, preventing localised deformations that commonly occur with other post-processing methods such as thermal treatments. The minimal dimensional changes and uniform deformation results demonstrate that the CIP process can effectively enhance the mechanical properties of sCFRP components while preserving dimensional stability.

4. Discussion

Mechanical and microstructural analysis of MEX-manufactured sCFRP components reveals distinct structural discontinuities inherent to the layer-by-layer deposition process. The primary structural limitations include void formation between layers, weak molecular bonding at interfaces, and directional fibre alignment along the printing path. Such structural features create significant mechanical anisotropy, leading to reduced strength in specimens printed in the 90° orientation due to the dominance of interlayer bonding over fibre reinforcement effects.

To overcome these structural limitations while avoiding thermal degradation, this study investigates cold isostatic pressing as a novel approach. The systematic investigation demonstrates the effectiveness of CIP treatment in enhancing the structural, mechanical, and thermal properties of sCFRP components through increased filament contact area and polymer chain mobility. The mechanical property improvements can be primarily result from structural modifications including void elimination, enhanced interfacial bonding, and modified fibre-matrix interactions. Additionally, pressure-induced changes in polymer crystallinity further enhance the overall performance. This section presents the process-structure–property relationship for MEX-manufactured and CIP-treated sCFRP through comprehensive analysis of mechanical properties (Section 4.1), crystallization behaviour

(Section 4.2), and pressure-induced bonding mechanisms (Section 4.3).

4.1. Mechanical characteristics

The mechanical behaviour of MEX-manufactured sCFRP specimens exhibited distinct characteristics based on raster angle orientation [59]. This raster angle-dependent tensile behaviour is theoretically described by the Tsai-Hill equation for fibre-reinforced composites [60]:

$$TS_c = \frac{\cos^4\theta}{\sigma_l^2} + \sin^2\theta\cos^2\theta \times \left(\frac{1}{\tau_m^2} - \frac{1}{\sigma_l^2}\right) + \frac{\sin^4\theta^-\frac{1}{2}}{\sigma_t^2} \quad (4)$$

where TS_c is the composite tensile strength, τ_m the matrix shear strength, θ the fibre orientation angle, σ_l the longitudinal stress ($\theta = 0°$), and σ_t the transverse stress ($\theta = 90°$).

According to this equation, when $\theta = 0°$ (fibres aligned with nozzle direction), the expression simplifies to $TS_c \approx \sigma_l$, indicating that longitudinal fibre properties dominate the mechanical response. At this orientation, CFs align parallel to the tensile loading direction, resulting in mechanical properties primarily determined by fibre characteristics [61]. In contrast, when $\theta = 90°$ (fibres perpendicular to loading direction), the expression becomes $TS_c \approx \sigma_t$, where transverse properties control the mechanical behaviour. At this 90° orientation, layers are perpendicular to the loading direction, causing mechanical properties to depend primarily on matrix properties and interlayer bonding strength [62]. The Tsai-Hill criterion explanation aligns with observations that specimens printed at 0° exhibit fibre-dominated properties while those at 90° are more sensitive to interlayer bonding quality and matrix properties.

The CIP treatment effectively addresses this anisotropy by preferentially enhancing matrix and interfacial properties that govern the transverse strength component, resulting in a more balanced mechanical performance between 0° and 90° orientations. At 500 bar, tensile strength increased from 73.4 to 149.3 MPa for 0° specimens, while 90° specimens showed improvement from 24.8 to 60.9 MPa. The more substantial improvement in 90° specimens (145% increase) compared to 0° specimens (104% increase) suggests that CIP treatment primarily enhances the matrix-dominated properties through improved interfacial bonding. The significant reduction in anisotropy from 66.2% to 49.3% at 250 bar demonstrates that CIP effectively addresses one of the fundamental limitations of MEX-manufactured components. Moreover, the CIP process required only 30 minutes, substantially shorter than traditional thermal processes.

To understand the underlying mechanisms responsible for the observed CIP-induced mechanical property enhancements, detailed analysis of the stress–strain behaviour and fracture morphology was conducted. As shown in Figure 9(a), untreated specimens with 0° raster angle exhibited linear elastic behaviour followed by brittle fracture due to air gaps generated during the MEX process. In contrast, CIP-treated specimens with 0° raster angle exhibited enhanced tensile strength through increased effective load-bearing capacity between layers. Morphological analysis revealed a transition from fibre pull-out to fibre breakage in fracture surfaces, indicating stronger interfacial adhesion and

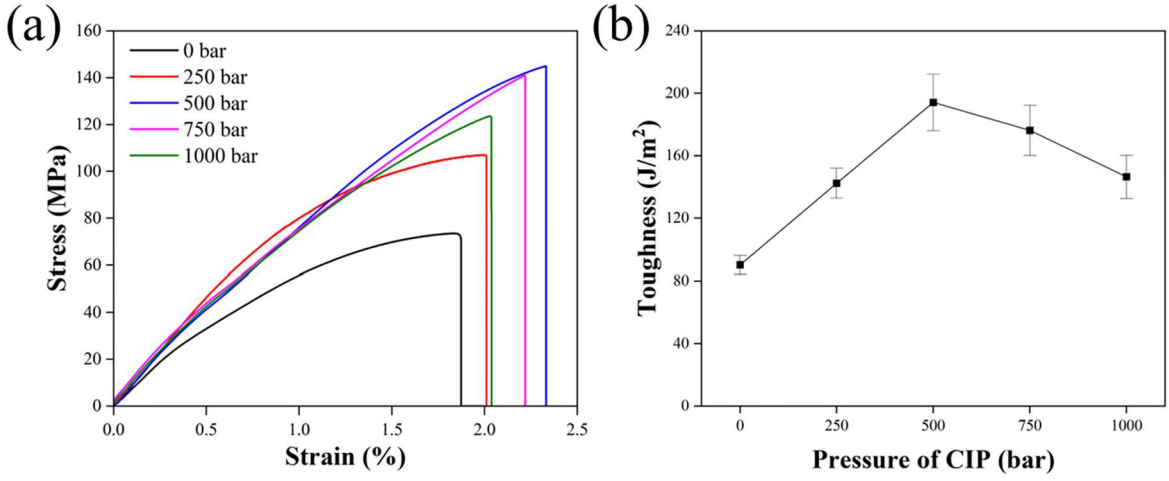

Figure 9. Mechanical behaviour analysis: (a) Representative stress–strain curves for specimens at different pressures, and (b) Toughness comparison of CIP-treated specimens.

more efficient load transfer between matrix and reinforcement. To quantify these improvements, specimen toughness was calculated and presented in Figure 9(b). CIP-treated specimens showed enhanced toughness compared to untreated specimens, with 0° specimens showing a 111% increase at 500 bar (194 J/m^2). According to crack propagation theory, the air gaps and weak fibre-matrix interfaces in untreated specimens act as preferential pathways for rapid crack propagation [63,64]. These pathways promote delamination between CF and matrix, resulting in premature failure where fibre pull-out dominates the fracture mechanism [65,66]. In contrast, in CIP-treated specimens, the strengthened fibre-matrix interfaces effectively redistribute stress concentrations, causing crack propagation to occur through CFs rather than along the fibre-matrix boundary.. This change in crack propagation behaviour explains the transition from fibre pull-out to fibre breakage observed in our samples. However, excessive isostatic pressure can introduce internal micro-cracks within the sCFRP structure. Excessive isostatic pressures generate internal micro-fractures that form localised stress concentration regions within the sCFRP structure, exhibiting brittle fracture characteristics which leads to diminished mechanical performance.

The effect of enhanced interfacial bonding through CIP was also observed in flexural and ILSS properties. As shown in Figure 5(a,b), flexural strength increased up to 500 bar, exhibiting a property degradation at higher pressures. The flexural modulus showed similar behaviour, reaching its maximum value at 500 bar, with decreased values observed at 750 and 1000 bar. The enhancement in flexural properties correlates with the microstructural modifications induced by isostatic pressure, particularly the reduction in void content and improved interfacial bonding. Similar trends were observed for ILSS strength. The ILSS reached its maximum value at 500 bar and decreased at higher pressures. To understand the mechanism behind these ILSS improvements, the relationship between pressure and interlayer bonding was analysed. The interlayer bond strength depends on polymer diffusion rate at the interface. The relationship between interlayer bond strength and molecular chain diffusion time is demonstrated by Equation (5):

$$\sigma_b \propto \left(\frac{t_d}{M_w}\right)^{\frac{1}{4}} \tag{5}$$

where t_d is the diffusion time, M_w is the molecular weight, and σ_b is the interlayer bond strength.

The enhanced ILSS in CIP-treated specimens indicates increased polymer chain diffusion between layers. Isostatic pressure application facilitates interfacial contact between adjacent layers, leading to accelerated polymer chain diffusion. Microstructural analysis reveals reduced layer spacing in CIP-treated specimens. This increased interfacial contact area promotes polymer chain diffusion across layers, resulting in improved interlayer bonding strength.

The mechanical test results summarised in Table 3 demonstrate comprehensive improvements in tensile, flexural, and ILSS properties through CIP treatment. However, application of excessive isostatic pressure led to mechanical property deterioration through internal microcrack formation and delamination during interlayer bonding. Microstructural analysis confirmed these pressure-dependent variations in mechanical properties, revealing CF agglomeration on the tensile fracture surface at excessive pressures (Figure 7(j)). Therefore, comprehensive control of MEX and post-processing parameters is essential to achieve optimal interlayer bond strength while minimising anisotropy in MEX-manufactured sCFRP components.

To provide a more comprehensive explanation of isostatic pressure-dependent mechanical behaviour, the theoretical analysis based on the modified Kelly-Tyson model was employed to evaluate the effects of CIP treatment on sCFRP components. The modified Kelly-Tyson model incorporates both end-region fibre stress distribution and void volume fraction parameters, which are critical microstructural characteristics of MEX-manufactured sCFRP composites.

According to the modified Kelly-Tyson model, the tensile strength of a short fibre-reinforced composite (σ_c) can be expressed as:

$$\sigma_c == \eta_0 \times (X + Y) + Z \tag{6}$$

where X, Y and Z denote the sub-critical fibre contribution, super-critical fibre contribution and modified

Table 3. Mechanical properties of CIP-treated specimens.

Specimens	Tensile strength [MPa]	Tensile modulus [GPa]	Flexural strength [MPa]	Flexural modulus [GPa]	ILSS [MPa]
0 bar	73.49 ± 0.01	7.20 ± 0.11	155.42 ± 1.78	11.08 ± 0.27	11.49 ± 0.54
250 bar	104.74 ± 2.38	8.72 ± 0.15	197.02 ± 0.70	15.03 ± 0.06	15.64 ± 1.08
500 bar	149.39 ± 4.49	10.17 ± 0.72	215.61 ± 11.20	15.08 ± 1.82	21.38 ± 0.48
750 bar	136.91 ± 4.04	8.84 ± 0.07	197.38 ± 4.08	13.48 ± 1.07	13.12 ± 0.08
1000 bar	120.07 ± 3.47	8.78 ± 0.14	198.01 ± 1.22	14.28 ± 0.58	13.24 ± 1.96

matrix contribution, respectively. Based on the iso-strain assumption $\varepsilon_c = \varepsilon_m = \varepsilon_f$, these terms can be written as:

$$X = \sum_{i}^{L_i<L_c} V_i \times \left(\frac{\tau_s \times L_i}{D} + \sigma_0\right) \tag{7}$$

$$Y = \sum_{j}^{L_j>L_c}\left[E_f \times \varepsilon_c \times V_j \times \left(1 - \frac{(E_f \times \varepsilon_c - \sigma_0)^2 \times D}{4E_f \times \varepsilon_c \times \tau_s \times L_j}\right)\right] \tag{8}$$

$$Z = E_m \times \varepsilon_c \times (1 - V_f - V_p) \tag{9}$$

where E_f is the fibre elastic modulus, E_m is the matrix elastic modulus, ε_c is the composite strain, τ_s is the interfacial shear strength, D is the fibre diameter, σ_0 is the stress at the fibre ends, L_i and L_j represent the lengths of sub-critical and super-critical fibres respectively, V_i and V_j are the corresponding volume fractions, V_f is the total fibre volume fraction, and V_p is the void volume fraction. The fibre orientation factor (η_0), which plays a critical role in this model, can be determined by:

$$\eta_0 = \frac{\sum_{i=1}^{n} \cos\theta_i}{n} \tag{10}$$

where θ_i represents the angle between each fibre and the loading direction, and n is the total number of fibres examined.

The modified Kelly-Tyson model provides a framework to explain the observed mechanical behaviour under different isostatic pressures. In the lower pressure range (0–500 bar), CIP treatment effectively reduces the void volume fraction as evidenced by the progressive reduction in voids observed in the SEM micrographs (Figure 6(c–f)). The reduction in V_p directly contributes to the mechanical strength enhancement through the Z term. Simultaneously, the improved interfacial bonding between fibre and matrix, confirmed by the significant increase in ILSS values, enhances the effective stress transfer parameter (τ) which positively influences both X and Y terms.

However, when the isostatic pressure exceeds 500 bar, microstructural examination reveals that fibre orientation begins to deviate from the originally aligned state produced during the MEX process. This randomisation decreases the fibre orientation factor (η_0), which has a multiplicative effect on both fibre contribution terms (X and Y) in Equation (9). Furthermore, the SEM analysis shows evidence of fibre agglomeration at higher pressures (Figures 6(i) and 7(j)), which creates localised stress concentration points and reduces the effective load-bearing capacity of the composite [67].

The trade-off between void reduction and deteriorating fibre orientation results in a mechanical property peak at 500 bar CIP pressure. This optimal pressure represents the specific processing condition where maximum void reduction is achieved while maintaining fibre orientation and distribution. These experimental findings are supported by consistent with the modified Kelly-Tyson model, which predicts that composite strength depends on the combined effects of fibre orientation, interfacial bonding, and void content. The mechanical effectiveness of the CIP-treated composites has been verified by the above tests and analyses. To evaluate the practical feasibility of CIP treatment, it needs to be compared to existing sCFRP composites. Figure 10(a) shows the mechanical properties of CIP-treated specimens compared to other reported sCFRP composites. Typically, PA-matrix composites containing 15 wt % CF exhibit tensile strengths ranging from 50 MPa to 80 MPa, with conventional sCFRP reaching up to 100 MPa. The CIP-treated specimens in this work achieved

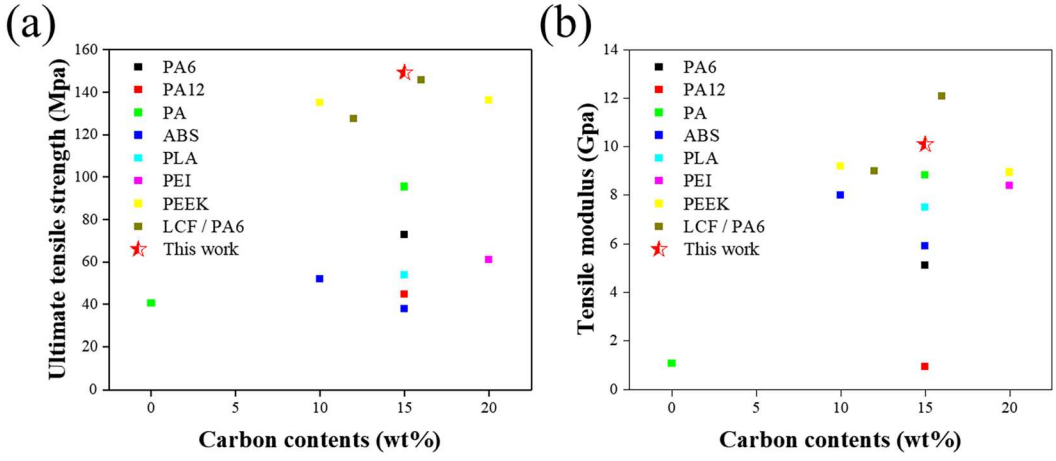

Figure 10. Comparison of mechanical properties between this study and literature data for various composites (a) tensile strength and (b) tensile modulus.

tensile strengths of approximately 150 MPa, surpassing even high-performance PEEK/CF composites. Figure 10(b) compares the tensile modulus between CIP-treated and conventional sCFRP at different fibre contents. While traditional sCFRP composites show limited mechanical properties due to insufficient consolidation, the CIP-treated specimens have demonstrated superior mechanical properties through better fibre and matrix integration. Specifically, the CIP-treated sCFRP in this study achieved a tensile modulus of approximately 10 GPa with 15 wt% sCF, surpassing the performance of sCFRP containing higher fibre content (20 wt% sCF).

In addition to mechanical properties, dimensional stability is another critical factor for practical applications. The dimensional stability of CIP-treated specimens was evaluated by comparing with various post-processing methods reported in literature. Table 4 presents the dimensional deformation rates for different materials and post-treatment techniques. Previous studies have reported significant dimensional changes in conventional post-processing methods, ranging from 10% to 19% deformation. In contrast, the CIP-treated sCFRP specimens in this work exhibited remarkably low dimensional changes of only 1∼4% (Figure 8), demonstrating enhanced dimensional stability compared to conventional post-processing methods. As shown in Figure 8(b,c), the dimensional changes remained minimal across different CIP pressures (250–1000 bar) for both flexural and ILSS specimens, confirming the superior capability of CIP treatment in preserving component geometry while improving interlayer bonding.

4.2. Crystalline behaviour

The significant improvements in mechanical properties across all specimens suggest underlying microstructural and crystallinity changes induced by CIP treatment. To understand the enhancement of CIP-treated specimens, crystalline behaviour was investigated through thermal analysis. As previously discussed in Section 3.2, both X_c and T_g showed systematic variation with applied pressure. In semi-crystalline polymers like PA, the molecular structure can transform from amorphous to crystalline states under specific pressure and temperature conditions [39].

During the initial CIP stage (0–250 bar), isostatic pressure induces a reduction in free volume between polymer chains, promoting initial molecular alignment. This molecular reorganisation creates favourable conditions for crystalline phase formation within the polymer matrix. As pressure increases to 500 bar, the maintained molecular alignment combined with enhanced molecular diffusion between layers facilitates stronger polymer chain formation through secondary bonding. The molecular chain reorganisation establishes thermodynamically stable configurations, resulting in optimal crystallinity. The increased T_g of 74.93° C at pressure condition of 500 bar reflects enhanced molecular chain rigidity, resulting in improved mechanical properties [57,69]. In contrast, pressure treatment above 500 bar leads to crystallinity deterioration. Microstructural analysis revealed that isostatic treatment above 750 bar resulted in CF agglomeration and random fibre orientation. However, this configuration fails to provide consistent nucleation sites for crystallization and compromises optimal load distribution. The resulting structural arrangement leads to reduced DOC, decreasing mechanical properties for primary loading directions.

Previous studies have shown that post-processing enhances the interfacial strength between fibre and matrix, leading to improved tensile strength and modulus [19]. Frenkel-Eshelby and Hooke's laws quantitatively validate that increased interfacial strength between layers directly correlates with improvements in tensile behaviours [40]. Therefore, the increased DOC through CIP treatment enhances the interfacial bonding between CF and matrix, contributing to the improved mechanical properties.

The enhanced interfacial bonding was verified through microstructural observation. The untreated specimen fracture surfaces exhibited fibre debonding, characteristic of weak interfacial bonding (Figure 11(a)). In contrast, the specimens treated at 500 bar displayed fibre breakage, signifying strong CF-matrix bonding (Figure 11(b)). The CIP process reveals an optimal pressure range where enhanced interfacial bonding is achieved through higher crystallinity, while excessive pressure leads to mechanical property deterioration. The mechanical property degradation is attributed to structural damage and the development of

Table 4. Comparison about dimensional deformation other literature.

Material	Method	Deformation	Ref
sCF / PEEK	Microwave annealing	Thickness increase: 10%	Ai, Li, and Vogt [68]
ABS	Warm isostatic pressing	Shrinkage: 18.9%	SeongJe Park et al. [41]
rCF / ABS	Annealing	Shrinkage: 18.8%	Seok, Jeon, and Kim [15]
PLA	Hot roller	z-direction deformation: 0.72 mm	Andreu et al. [29]
S-CCFRC	Annealing	Width deformation: 16.74%	Wang et al. [37]
sCF / PA	CIP	Width deformation: 4% Thickness deformation: 1%	This work

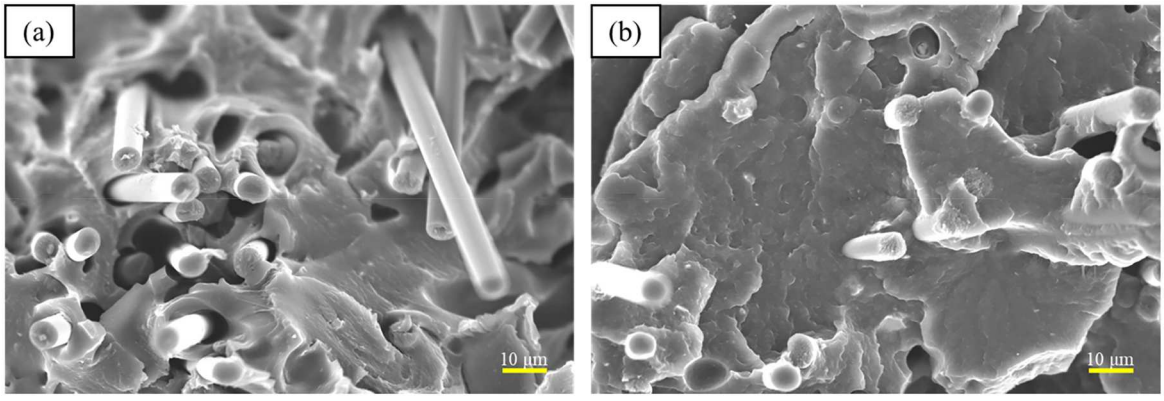

Figure 11. Microstructural comparison of the fibre–matrix interface: (a) Fibre pull-out in the untreated specimen and (b) Fibre breakage in CIP-treated specimen at 500 bar.

large crystal structures restricting molecular chain mobility, thereby reducing material ductility [70]. Optimising the CIP treatment conditions requires balancing the isostatic pressure effects on mechanical strength and material ductility.

The analysis of isostatic pressure effects on crystallization behaviour reveals that CIP promotes crystalline structure formation through pressure-induced chain alignment at room temperature. The CIP crystallization approach offers distinct advantages over conventional thermal processes. This room-temperature method provides enhanced control over crystallization while preventing thermal degradation and dimensional instability. These crystallinity observations provide important insights into the mechanical behaviour explained by the modified Kelly-Tyson model discussed in Section 4.1. The progressive increase in X_c up to 500 bar (from 26.82% to 30.43%) enhances the interfacial shear strength parameter (τ_s), leading to improved stress transfer efficiency at the fibre-matrix interface. Furthermore, the increased crystallinity contributes to higher matrix tensile strength, positively affecting the matrix contribution.

4.3. Effect of isostatic pressure

The experimental results demonstrate that CIP post-processing effectively addresses the inherent limitations of MEX-manufactured sCFRP components. The systematic analysis of mechanical properties, crystallinity changes, and microstructural modifications reveals the mechanisms responsible for property enhancement through CIP treatment.

As shown in Figure 12(a), polymer interface bond formation during conventional thermal treatment occurs in four stages [71]:

(i) surface contact involving localized polymer flow and molecular movement at the interface, (ii) close physical contact between two interfaces (neck growth), (iii) molecular diffusion and randomization across the entire interface (molecular diffusion), and (iv) the gradual cooling of the interface (cooling). However, heat treatment methods require high temperatures to enhance polymer diffusion between layers. These conventional treatments result in slow molecular diffusion rates and potential polymer softening. In contrast, the CIP process enhances interfacial contact between layers through high isostatic pressure application, promoting molecular chain mobility and gradual coalescence at filament interfaces. This study proposes that CIP enhances molecular entanglement across amorphous and crystalline regions, which improves both interlayer adhesion and material crystallinity. As shown in Figure 12(b), the behavior of amorphous and crystalline regions during CIP proceeds in four stages: (i) the void volume between interfaces decreases, and surface contact begins during the initial application of isostatic pressure (initial contact), as observed in Section 3.3, (ii) the physical contact area between interfaces expands, and molecular chain rearrangement begins as pressure increases (contact area widen) [57,69], (iii) molecular chain entanglement occurs, and crystalline regions reorganize at maximum pressure (intermolecular bonding), and (iv) the formed molecular bonds and rearranged structures are maintained and stabilized upon pressure removal (structure stabilization), as presented in Section 3.1. Consequently, the CIP process achieves efficient interlayer bonding while maintaining the dimensional stability of MEX-manufactured components at room temperature. This enhancement is quantitatively validated by improved mechanical properties and observed microstructural changes after CIP treatment, as well as the modified Kelly-Tyson model discussed in Section 4.1, which demonstrates that the increased crystallinity directly enhances the interfacial shear strength

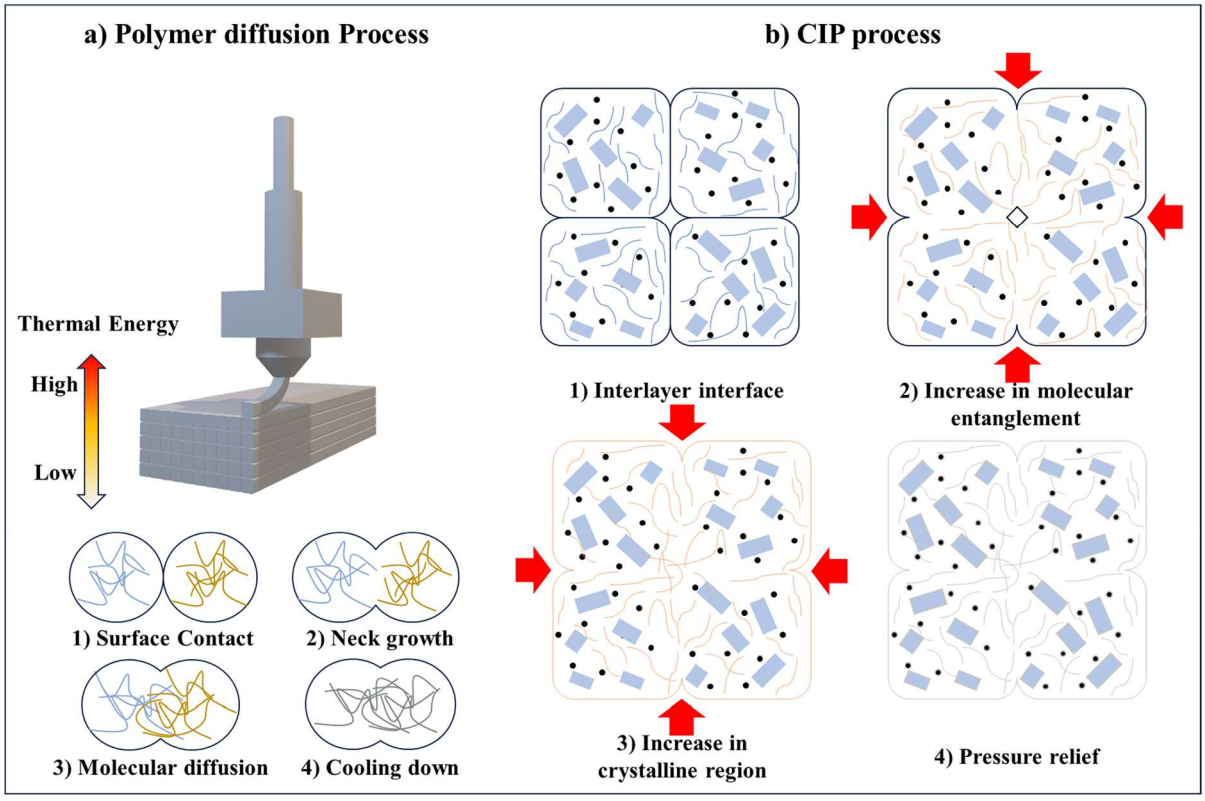

Figure 12. Schematic representation of bonding mechanism: (a) conventional thermal bonding process and (b) proposed CIP bonding mechanism in four stages.

parameter (τ_s), resulting in more efficient stress transfer at the fiber-matrix interface.

The room-temperature CIP process overcomes limitations of conventional thermal post-processing methods, particularly polymer degradation and dimensional instability. The absence of thermal activation eliminates issues related to differences in thermal expansion coefficients between fibre and matrix, while achieving significant improvements in interfacial bonding and mechanical properties.

5. Conclusions

This study investigated the effects of CIP post-processing on the mechanical properties of MEX-manufactured sCFRP composites. To assess the effect of CIP on MEX-manufactured sCFRP components, various isostatic pressures (250–1000 bar) were applied during CIP treatment. Mechanical, thermal, and microstructural analyses were conducted to systematically evaluate the pressure-dependent effects on the composites.

The key findings of this study include:

- Optimal CIP pressure of 500 bar produced maximum mechanical enhancements: 103% tensile strength, 40.9% flexural strength, and 82.7% interlaminar shear strength.
- Mechanical anisotropy of MEX-manufactured composites reduced from 66.2% to 49.3%.
- Crystallinity increased by 12.4% (from 26.8% to 30.4%).

Microstructural analysis revealed that the CIP treatment effectively reduced the interlayer and interfilament voids while increasing the contact area, serving as the primary mechanism for enhancing the mechanical properties. The dimensional stability analysis showed minimal shape deformation after CIP treatment (maximum deformation rate of 3%), demonstrating superior dimensional stability compared with conventional thermal treatment methods. CIP demonstrated significant potential as a room-temperature post-processing method for MEX-manufactured sCFRP components, without thermal degradation while requiring only 30 min of processing time compared to several hours for traditional thermal treatments. The CIP process provides an effective post-processing method for MEX-manufactured sCFRP composites by enhancing mechanical properties through pressure-induced molecular diffusion without thermal degradation. This room-temperature process offers significant advantages over

conventional thermal treatments, particularly for semi-crystalline polymers. While the results demonstrate considerable improvement in mechanical properties, the current study is limited to static mechanical testing and semi-crystalline polymer matrix composites only. Future research will focus on investigating the long-term durability of CIP-treated composites under various environmental exposures and dynamic performance under cyclic loading conditions. Further investigations will include comprehensive testing across various fibre volume fractions, detailed analysis of interface characteristics as a function of pressure and holding time. These investigations are expected to facilitate the implementation of CIP-treated composites in demanding applications across aerospace, automotive, and industrial sectors.

Disclosure statement

No potential conflict of interest was reported by the author(s).

Funding

This research was supported by the Ministry of Trade, Industry and Energy (MOTIE, Korea) through the 2025 R&D HRD Program for Problem-Solving Based on Future Mobility Innovation Technology Development (Project No. P0023726) and This work was also supported by the National Research Foundation of Korea (NRF) grant funded by the Korea government (MSIT) (IRIS RS-2025-00558176).

Data availability statement

The raw data supporting the findings of this study are available on the web. https://github.com/sangjune-jeon/Cold-Isostatic-Press.

References

[1] Koord J, Hühne C. Effect of low temperature on interlaminar fracture toughness of multi-directional CFRP and CFRP-steel interfaces. Compos B Eng. 2024;281(July):111540. doi:10.1016/j.compositesb.2024.111540

[2] Garulli T, Katafiasz TJ, Greenhalgh ES, et al. A novel bio-inspired microstructure for improved compressive performance of multidirectional CFRP laminates. Compos B Eng. 2023;264(September):110867. doi:10.1016/j.compositesb.2023.110867

[3] Yavas D, Zhang Z, Liu Q, et al. Interlaminar shear behavior of continuous and short carbon fiber reinforced polymer composites fabricated by additive manufacturing. Compos B Eng. 2021;204(January):108460. doi:10.1016/j.compositesb.2020.108460

[4] Khan F, Hossain N, Mim JJ, et al. Advances of composite materials in automobile applications – a review. J Eng Res. 2024;February; doi:10.1016/j.jer.2024.02.017

[5] Lee J-M, Min B-J, Park J-H, et al. Design of lightweight CFRP automotive part as an alternative for steel part by thickness and lay-up optimization. Materials (Basel). 2019;12(14). Multidisciplinary Digital Publishing Institute:2309. doi:10.3390/ma12142309

[6] Li A, Mao Q, Li J, et al. Review on methodologies of fatigue property prediction for carbon fiber reinforced polymer. Compos B Eng. 2024;284(September):111659. doi:10.1016/j.compositesb.2024.111659

[7] Geier N, Xu J, Poór DI, et al. A review on advanced cutting tools and technologies for edge trimming of carbon fibre reinforced polymer (CFRP) composites. Compos B Eng. 2023;266(November):111037. doi:10.1016/j.compositesb.2023.111037

[8] Geier N, Patra K, Anand RS, et al. A critical review on mechanical micro-drilling of glass and carbon fibre reinforced polymer (GFRP and CFRP) composites. Compos B Eng. 2023;254(April):110589. doi:10.1016/j.compositesb.2023.110589

[9] Zhang J, Lin G, Vaidya U, et al. Past, present and future prospective of global carbon fibre composite developments and applications. Compos B Eng. 2023;250(February):110463. doi:10.1016/j.compositesb.2022.110463

[10] Liu W, Huang H, Zhu L, et al. Integrating carbon fiber reclamation and additive manufacturing for recycling CFRP waste. Compos B Eng. 2021;215(June):108808. doi:10.1016/j.compositesb.2021.108808

[11] Khosravani MR, Berto F, Ayatollahi MR, et al. Fracture behavior of additively manufactured components: A review. Theor Appl Fract Mech. 2020;109(October):102763. doi:10.1016/j.tafmec.2020.102763

[12] Heidari-Rarani M, Rafiee-Afarani M, Zahedi AM. Mechanical characterization of FDM 3D printing of continuous carbon fiber reinforced PLA composites. Compos B Eng. 2019;175(October):107147. doi:10.1016/j.compositesb.2019.107147

[13] Wang P, Wen J, Lei H, et al. Morphology characterization and *in-situ* three-dimensional strain field monitor of short carbon fiber-reinforced polymer composites under tension. Compos Struct. 2021;262(April):113634. doi:10.1016/j.compstruct.2021.113634

[14] Yamaguchi A, Uematsu H, Sakaguchi T, et al. Effects of different types of functionalized polypropylenes on the tensile strength of short carbon fiber-reinforced polypropylene composites. Polym J. 2024;56(3). Nature Publishing Group:205–214. doi:10.1038/s41428-023-00856-8

[15] Seok W, Jeon E, Kim Y. Effects of annealing for strength enhancement of FDM 3D-printed ABS reinforced with recycled carbon fiber. Polymers (Basel). 2023;15(14). Multidisciplinary Digital Publishing Institute:3110. doi:10.3390/polym15143110

[16] Garmabi MM, Shahi P, Tjong J, et al. 3D printing of polyphenylene sulfide for functional lightweight automotive component manufacturing through enhancing interlayer bonding. Addit Manuf. 2022;56(August):102780. doi:10.1016/j.addma.2022.102780

[17] Gao X, Qi S, Kuang X, et al. Fused filament fabrication of polymer materials: a review of interlayer bond. Addit Manuf. 2021;37(January):101658. doi:10.1016/j.addma.2020.101658

[18] Sultan R, Skrifvars M, Khalili P. 3D printing of polypropylene reinforced with hemp fibers: mechanical, water absorption and morphological properties. Heliyon. 2024;10(4):e26617. doi:10.1016/j.heliyon.2024.e26617

[19] Park SJ, Kim DH, Ju HG, et al. Increased interlayer bonding strength of short carbon fiber composite fabricated by material extrusion via warm isostatic pressing (WIP) process. J Mater Res Technol. 2023;25(July):3610–3623. doi:10.1016/j.jmrt.2023.06.130

[20] Wu J, Zhang K, Yang D. Material extrusion additive manufacturing of recycled discontinuous carbon fibre reinforced thermoplastic composites with different fibre lengths: through-process microstructural evolution and mechanical property loss. Addit Manuf. 2023;78(September):103839. doi:10.1016/j.addma.2023.103839

[21] Bu H, Zhan X, Hu Z, et al. Enhanced interlayer strength in 3D-printed PA12 composites via electromagnetic induction post-processing. Addit Manuf. 2024;92(July):104383. doi:10.1016/j.addma.2024.104383

[22] Mehdikhani M, Gorbatikh L, Verpoest I, et al. Voids in fiber-reinforced polymer composites: a review on their formation, characteristics, and effects on mechanical performance. J Compos Mater. 2019;53(12). SAGE Publications Ltd STM:1579–1669. doi:10.1177/0021998318772152

[23] Wang L, Jiang J, Dong Y, et al. Machine learning enabled 3D printing parameter settings for desired mechanical properties. Virtual Phys Prototyp. 2024;19 (1). doi:10.1080/17452759.2024.2425825

[24] Ivorra-Martinez J, Peydro MÁ, Gomez-Caturla J, et al. The effects of processing parameters on mechanical properties of 3D-printed polyhydroxyalkanoates parts. Virtual Phys Prototyp. 2023;18 (1). doi:10.1080/17452759.2022.2164734

[25] Liaw C-Y, Tolbert JW, Chow LW, et al. Interlayer bonding strength of 3D printed PEEK specimens. Soft Matter. 2021;17(18). The Royal Society of Chemistry:4775–4789. doi:10.1039/D1SM00417D

[26] Gómez-Ortega A, Piedra S, Mondragón-Rodríguez GC, et al. Dependence of the mechanical properties of nylon-carbon fiber composite on the FDM printing parameters. Compos Part A Appl Sci Manuf. 2024;186(November):108419. doi:10.1016/j.compositesa.2024.108419

[27] Rimašauskas M, Jasiūnienė E, Kuncius T, et al. Investigation of influence of printing parameters on the quality of 3D printed composite structures. Compos Struct. 2022;281(February):115061. doi:10.1016/j.compstruct.2021.115061

[28] Qu Z, Zhang Z, Liu R, et al. High fatigue resistance in a titanium alloy via near-void-free 3D printing. Nature. 2024;626(8001). Nature Publishing Group:999–1004. doi:10.1038/s41586-024-07048-1

[29] Andreu A, Kim S, Dittus J, et al. Hybrid material extrusion 3D printing to strengthen interlayer adhesion through Hot rolling. Addit Manuf. 2022;55(July):102773. doi:10.1016/j.addma.2022.102773

[30] Wang Z, Zhang B, Wang J. Influences of isothermal annealing post-treatment on mechanical performances in fused deposition modeling manufactured short carbon fibrous PETG and PA composites. Polym Eng Sci. 2024;64(12):6247–6264. doi:10.1002/pen.26984

[31] Braconnier DJ, Dunn RM, Wetzel ED, et al. The role of crystallization and annealing on the thermal conductivity of material extrusion additively manufactured parts. Addit Manuf. 2024;89(June):104265. doi:10.1016/j.addma.2024.104265

[32] Lin Z, Guo R, Lyu Y, et al. Enhanced interlayer adhesion and regulated tribological behaviors of 3D printed poly(Ether Ether Ketone) by annealing. Tribol Int. 2025;202(February):110362. doi:10.1016/j.triboint.2024.110362

[33] Nguyen KQ, Vuillaume PY, Hu L, et al. Effect of in situ thermal treatment on interlayer adhesion of 3D printed polyetherimide (PEI) parts produced by fused deposition modeling (FDM). Mater Today Commun. 2024;39(June):108588. doi:10.1016/j.mtcomm.2024.108588

[34] Yu N, Sun X, Wang Z, et al. Effects of auxiliary heat on the interlayer bonds and mechanical performance of polylactide manufactured through fused deposition modeling. Polym Test. 2021;104(December):107390. doi:10.1016/j.polymertesting.2021.107390

[35] He Y, Shen M, Wang Q, et al. Effects of FDM parameters and annealing on the mechanical and tribological properties of PEEK. Compos Struct. 2023;313(June):116901. doi:10.1016/j.compstruct.2023.116901

[36] Wang P, Zou B. Improvement of heat treatment process on mechanical properties of FDM 3D-printed short- and continuous-fiber-reinforced PEEK composites. Coatings. 2022;12(6). Multidisciplinary Digital Publishing Institute:827. doi:10.3390/coatings12060827

[37] Wang K, Long H, Chen Y, et al. Heat-Treatment effects on dimensional stability and mechanical properties of 3D printed continuous carbon fiber-reinforced composites. Compos Part A Appl Sci Manuf. 2021;147(August):106460. doi:10.1016/j.compositesa.2021.106460

[38] Wang J, Tan Q, Wang K, et al. A heat-press-treatment method for 3D printed thin-walled composite structures with improved interfacial and compressive properties. Polym Compos. 2022;43(11):8471–8482. doi:10.1002/pc.27017

[39] Wu W, Xin J, Hu B, et al. Achieving injection molding interlayer strength via powder assisted Hot isostatic pressing in material extrusion polyetheretherketone. Addit Manuf. 2023;74(July):103735. doi:10.1016/j.addma.2023.103735

[40] Park SJ, Park SJ, Son Y, et al. Influence of warm isostatic press (WIP) process parameters on mechanical properties of additively manufactured acrylonitrile butadiene styrene (ABS) parts. Int J Adv Manuf Technol. 2022;122(7):3311–3322. doi:10.1007/s00170-022-10094-6

[41] Park SJ, Park SJ, Son Y, et al. Reducing anisotropy of a part fabricated by material extrusion via warm isostatic pressure (WIP) process. Addit Manuf. 2022;55(July):102841. doi:10.1016/j.addma.2022.102841

[42] Mei H, Ali Z, Yan Y, et al. Influence of mixed isotropic fiber angles and Hot press on the mechanical properties of 3D printed composites. Addit Manuf. 2019;27(May):150–158. doi:10.1016/j.addma.2019.03.008

[43] Attia UM. Cold-Isostatic pressing of metal powders: a review of the technology and recent developments. Crit Rev Solid State Mater Sci. 2021;46(6). Taylor & Francis:587–610. doi:10.1080/10408436.2021.1886043

[44] Solechan S, Suprihanto A, Widyanto SA, et al. Characterization of PLA/PCL/nano-hydroxyapatite (nHA) biocomposites prepared via cold isostatic pressing. Polymers (Basel). 2023;15(3). Multidisciplinary Digital Publishing Institute:559. doi:10.3390/polym15030559

[45] Yang W, Cai Z, Duan W, et al. Effect of feedstock bimodal powder design and cold isostatic pressing on the mechanical behavior of binder jetting additive manufactured inconel 718 superalloy. J Manuf Process. 2025;133(January):607–622. doi:10.1016/j.jmapro.2024.11.085

[46] Graham SJ, Azakli Y, Withey J, et al. CIP-FAST: assessing the production of complex geometry titanium components from powders by combining cold isostatic pressing (CIP) and field assisted sintering technology (FAST). Powder Metall. 2023;66(5). SAGE Publications:482–492. doi:10.1080/00325899.2023.2236907

[47] Zhu S, Xu B, Zhao W, et al. Enhancing flame retardancy in 3D printed polyamide composites using directionally arranged recycled carbon fiber. Compos B Eng. 2024;287(December):111854. doi:10.1016/j.compositesb.2024.111854

[48] Kepenekci M, Gharehpapagh B, Yaman U, et al. Mechanical performance of carbon fiber-reinforced polymer cellular structures manufactured via fused filament fabrication. Polym Compos. 2023a;44(8):4654–4668. doi:10.1002/pc.27429

[49] Kepenekci M, Gharehpapagh B, Yaman U, et al. Mechanical performance of carbon fiber-reinforced polymer cellular structures manufactured via fused filament fabrication. Polym Compos. 2023b;44(8):4654–4668. doi:10.1002/pc.27429

[50] Belei C, Pommer R, Amancio-Filho ST. Optimization of additive manufacturing for the production of short carbon fiber-reinforced polyamide/Ti-6Al-4V hybrid parts. Mater Des. 2022;219(July):110776. doi:10.1016/j.matdes.2022.110776

[51] Sadaghian H, Khalilzadehtabrizi S, Farzam M, et al. Behavior of 3D-printed polymers under monotonic torsion – a database of 15 different materials. Addit Manuf. 2022;60(December):103251. doi:10.1016/j.addma.2022.103251

[52] Park SJ, Choi JW, Park SJ, et al. Improving properties of a part fabricated by polymer-based powder bed fusion using a warm isostatic press (WIP) process. Materials & Design 2024;224(December):111417. doi:10.1016/j.matdes.2022.111417

[53] Hacioglu F, Tayfun U, Ozdemir T, et al. Characterization of carbon fiber and glass fiber reinforced polycarbonate composites and their behavior under gamma irradiation. Prog Nucl Energy. 2021;134(April):103665. doi:10.1016/j.pnucene.2021.103665

[54] Xu Z, Zou B, Ding S, et al. Study on the Hot isostatic pressing post-treatment of FDM-3D printed continuous carbon fiber reinforced composites. J Manuf Process. 2023;104(October):205–217. doi:10.1016/j.jmapro.2023.08.060

[55] Liesenfeld J, Jablonski JJ, Da Silva JRF, et al. Impact of annealing on the characteristics of 3D-printed graphene-reinforced PLA composite. J Manuf Process. 2024;128(October):133–157. doi:10.1016/j.jmapro.2024.08.025

[56] Yang D, Cao Y, Zhang Z, et al. Effects of crystallinity control on mechanical properties of 3D-printed short-carbon-fiber-reinforced polyether ether ketone composites. Polym Test. 2021;97(May):107149. doi:10.1016/j.polymertesting.2021.107149

[57] Rodzeń K, Harkin-Jones E, Wegrzyn M, et al. Improvement of the layer-layer adhesion in FFF 3D printed PEEK/carbon fibre composites. Compos Part A Appl Sci Manuf. 2021;149(October):106532. doi:10.1016/j.compositesa.2021.106532

[58] Lu S, Zhang B, Niu J, et al. High-Strength carbon fiber-reinforced polyether-ether-ketone composites with longer fiber retention length manufactured via screw extrusion-based 3D printing. Addit Manuf. 2024;86(April):104200. doi:10.1016/j.addma.2024.104200

[59] Ghabezi P, Sam-Daliri O, Flanagan T, et al. Upcycling waste polypropylene with basalt fibre reinforcement enhancing additive manufacturing feedstock for advanced mechanical performance. Appl Mater Today. 2024;41(December):102486. doi:10.1016/j.apmt.2024.102486

[60] Bandinelli F, Scapin M, Peroni L. Effects of anisotropy and infill pattern on compression properties of 3D printed CFRP: mechanical analysis and elasto-plastic finite element modelling. Rapid Prototyp J. 2024;30(11). Emerald Publishing Limited:142–158. doi:10.1108/RPJ-11-2023-0385

[61] Srinivasan Ganesh Iyer S, Keles O. Effect of raster angle on mechanical properties of 3D printed short carbon fiber reinforced acrylonitrile butadiene styrene. Compos Commun. 2022;32(June):101163. doi:10.1016/j.coco.2022.101163

[62] Forés-Garriga A, Pérez MA, Gómez-Gras G, et al. Role of infill parameters on the mechanical performance and weight reduction of PEI ultem processed by FFF. Mater Des. 2020;193(August):108810. doi:10.1016/j.matdes.2020.108810

[63] Chueca de Bruijn A, Gómez-Gras G, Fernández-Ruano L, et al. Optimization of a combined thermal annealing and isostatic pressing process for mechanical and surface enhancement of ultem FDM parts using doehlert experimental designs. J Manuf Process. 2023;85(January):1096–1115. doi:10.1016/j.jmapro.2022.12.027

[64] Song H, He G, He Y, et al. Effects of surface modification on mechanical properties and electromagnetic interference shielding properties of carbon fiber/silk fiber hybrid composites. Polym Compos. 2024;45(11):10276–10289. doi:10.1002/pc.28472

[65] Huang L, He Y, Gao Z, et al. Hybrid-Structured carbon fiber fabric/silk fiber non-woven fabric/carbonyl iron powder/epoxy composites with highly efficient electromagnetic interference shielding and mechanical properties. Compos Sci Technol. 2024;258(November):110868. doi:10.1016/j.compscitech.2024.110868

[66] Bermudo Gamboa C, Martín-Béjar S, Vilches JT, et al. Influence of printing parameters and short carbon fibre reinforcement on fatigue behaviour, dimensional accuracy and macrogeometrical deviations of polylactic acid in material extrusion. Compos Sci Technol. 2023;242(September):110205. doi:10.1016/j.compscitech.2023.110205

[67] He Y, Chen Q, Wu D, et al. Effect of multiscale reinforcement by fiber surface treatment with polyvinyl alcohol/graphene oxide/oxidized carbon nanotubes on the mechanical properties of reinforced hybrid fiber composites. Compos Sci Technol. 2021;204(March):108634. doi:10.1016/j.compscitech.2020.108634

[68] Ghabezi P, Sam-Daliri O, Flanagan T, et al. Circular economy innovation: a deep investigation on 3D printing of industrial waste polypropylene and carbon fibre composites. Resour Conserv Recycl. 2024;206(July):107667. doi:10.1016/j.resconrec.2024.107667

[69] Ai J-R, Li S, Vogt BD. Increased strength in carbon-poly(-ether ether ketone) composites from material extrusion with rapid microwave post processing. Addit Manuf. 2022;60(December):103209. doi:10.1016/j.addma.2022.103209

[70] Lv X, Yang S, Pei X, et al. Enhanced mechanical and tribological properties of 3D printed short carbon fiber reinforced polyether ether ketone composites. Polym Compos. 2024;45(10):8840–8860. doi:10.1002/pc.28380

[71] Yu W, Wang X, Yin X, et al. The effects of thermal annealing on the performance of material extrusion 3D printed polymer parts. Mater Des. 2023;226(February):111687. doi:10.1016/j.matdes.2023.111687

[72] Kim YH, Wool RP. A theory of healing at a polymer-polymer interface. Macromolecules. 1983;16(7):1115–1120. doi:10.1021/ma00241a013